Acknowledgment

This work was partially supported by the Brazilian Council for Scientific and Technological Research (CNPq) under Grant 300.682/93-0.

References

[1]Landahl, M. T., *Unsteady Transonic Flow*, Pergamon, Oxford, 1961, pp. 7–21.

[2]Runyan, H. L., and Woolston, D. S., "Method for Calculating the Aerodynamic Loadings on Oscillating Finite Wing in Subsonic and Sonic Flow," NACA Rept. 1322, 1957.

[3]Rodemich, E. R., and Andrew, L. V., "Unsteady Aerodynamics for Advanced Configurations, Part II—A Transonic Box Method for Planar Lifting Surfaces," U. S. Air Force Research Lab., FDL-TRD-64-152, Pt. II, Wright–Patterson AFB, OH, May 1965.

[4]Yates, E. C., Jr., "Unsteady Transonic Flow—Introduction, Current Trends, Applications," *Computational Methods in Potential Aerodynamics*, Springer-Verlag, Berlin, 1985, pp. 502–568.

[5]Soviero, P. A. O., and Pinto, F. H. L., "Unsteady Lifting Surface Theory in Sonic Flow: The Problem Revisited," *AIAA Journal*, Vol. 38, No. 5, 2000, pp. 931–933.

[6]Abramowitz, M., and Stegun, I. A. (eds.), *Handbook of Mathematical Functions, with Formulas, Graphs, and Mathematical Tables*, 9th ed., Dover, New York, 1970, p. 892.

[7]Davies, D. E., "Three Dimensional Sonic Flow Theory," *AGARD Manual on Aeroelasticity*, Pt. 2, 1960, Chap. 4, pp. 74–76.

A. Plotkin
Associate Editor

Effects of Changing Aspect Ratio Through a Wind-Tunnel Contraction

John Callan* and Ivan Marusic†
University of Minnesota, Minneapolis, Minnesota 55455

I. Introduction

ALMOST all high-quality wind tunnels use a contraction section to accelerate the flow into the working section. Obviously, the design of the contraction shape is crucial for producing the desired low-turbulence, uniform exit stream. Most present-day design rules are based on theoretical and computational studies that consider inviscid irrotational flow, and perhaps the best known of these is the study of Morel.[1] Morel analyzed contractions with an axisymmetric geometry and produced a series of design charts, giving the designer a tool for optimizing contraction length, contraction ratio, and curve shape based on the criteria of the possibility of separation in the contraction, along with the exit flow nonuniformity. It was concluded that the best contraction shapes were curves consisting of two matched cubic arcs whose match point is a varying parameter.

Although the majority of previous studies have concentrated on axisymmetric contractions, most wind-tunnel contractions are not axisymmetric but rather are three dimensional with rectangular cross-section. In this case an important parameter is the aspect ratio, denoted by AR and defined as the width/height at a given position in the contraction. One numerical study that has considered the design of three-dimensional contractions is that of Su,[2] who computed solutions to the three-dimensional Laplace equation. Based on the Morel criteria,[1] Su showed[2] that three-dimensional contractions exhibit poorer qualities, in terms of the possibility of flow separation and exit flow nonuniformity, than axisymmetric contractions with similar geometric properties (contraction ratio, etc.). The explanation given is that the presence of corners in the three-dimensional case produces greater velocity extrema than in the axisymmetric case. A feature that is present in three-dimensional contractions and not in axisymmetric ones is the effect of crossflow in the contraction. Su showed that the crossflow is induced due to the transverse pressure gradient existing in the contraction. This pressure gradient exists because of greater local velocity extrema at the corners relative to the centerline velocities on the walls on the planes of symmetry. A crossflow parameter was considered that showed the relative strengths of the crossflow effect for different contraction designs. No conjecture was attempted, however, on the effect of this crossflow on the flow quality at the exit, specifically on its effect on boundary-layer development. Su performed a parametric study by varying the important design parameters and studying their effect on the criteria set out by Morel.[1]

These previous studies, and others,[3,4] have focused on the numerical solution to the flow in the contraction for use as a tool for predicting the flow quality at exit. One study, that of Tulapurkara and Bhalla,[5] performed an experimental analysis of the flow in a contraction, in an attempt to verify Morel's predictions.[1] No studies, however, have focused on the actual flow in the working section at the exit of a contraction and the effect of changing the geometric parameters of the contraction on it. Furthermore, no previous studies have looked at the role that changing the AR through the length of the contraction has on the corner boundary layers. In the absence of any studies, designers have generally relied on rules of thumb to guide them. One of these is the so-called pyramid rule (A. E. Perry, private communication, 1997), which states that AR should be held constant throughout the contraction to minimize the growth of the corner boundary-layer vortices into the working section of the wind tunnel. This rule conflicts with the conclusion of Su[2] that changing AR can be advantageous when separation criteria are considered. However, because Su's study is based on solutions to potential flow, no rational comparison can be made. Maintaining a constant AR through the length of the contraction can often be impractical because of space constraints and also becomes a trade-off between varying other important parameters such as a higher contraction ratio, for example.

In this Note, we address the issue of changing the AR through a contraction by keeping inlet AR fixed at 1 and varying exit AR, while keeping the shape, contraction ratio, and length fixed. In this way, we can perform a parametric study of changing AR effects while keeping all other important parameters constant.

II. Experimental Procedure

Four contractions were constructed and were fitted to an existing wind-tunnel facility, each with fixed values for the various geometric parameters, with the exception of exit AR. The values of the fixed parameters are given in Table 1. As indicated in Table 1, the length of the contraction is denoted as L, A_i and A are the cross-sectional areas of the inlet and exit of the contraction respectively, and D_i and D are the inlet and exit effective diameters, respectively, where $D = (4A/\pi)^{1/2}$. The shape of the contraction surfaces are matched cubic arcs (following Morel[1] and Su[2]), where x_m is the distance from the beginning of the contraction to the match point of the cubic curves. The exit AR variation is given in Table 2.

Full details of the design and construction of the contractions are given by Callan.[6] In all cases, a short working section was attached to the exit of the contraction. Streamwise velocity and turbulence intensity measurements were made with a single component hot wire, one effective exit diameter downstream of the contraction exit. Data were gathered across the plane with the wires oriented both parallel

Table 1 Fixed parameters in study

Parameter	Value
Inlet area A_i, mm^2	600×600
Contraction ratio A_i/A	8.72
Contraction length/inlet effective diameter L/D_i	1.0
Contraction length L, mm	685
Cubic match point x_m/L	0.6
Exit Reynolds number $Re = U_e D/\nu$	4.8×10^5

Received 24 October 2000; revision received 4 June 2001; accepted for publication 4 June 2001.

*Research Assistant, Department of Aerospace Engineering and Mechanics.

†Assistant Professor, Department of Aerospace Engineering and Mechanics. Member AIAA.

Table 2 Exit aspect ratios considered

AR	Exit dimensions, mm^2
1	203 × 203
2.3	305 × 135
3.1	356 × 116
4	406 × 102

to the floor and parallel to the side wall. In addition, boundary-layer profiles on the centerlines of the floor and side wall, respectively, were obtained using the hot wires. Following the study of Zamir and Young,[7] corner boundary layer profiles were obtained with the wire oriented perpendicular to the 45-deg axis of the corner.

For all measurements, 5-μm single Wollaston wires were used, with an etched length of nominally 1 mm. A TSI IFA-100 anemometer was operated with an overheat ratio of 1.8, and the signals were conditioned and digitized with 16-bit resolution. The hot wires were calibrated statically using a third-order polynomial curve fit. Measurements are estimated to be accurate to within ±2% for mean velocity and ±4% for the turbulence intensities.

III. Results and Discussion

A. Convergence Parameter

A principal feature of the effect of AR change through a contraction is its effect on the development of the boundary layers on the walls and in the corners of the contraction. Bradshaw[8] shows that boundary-layer development is controlled not only by streamwise pressure gradients, but also by the effect of the extra straining caused by a diverging or converging flow. Following Saddoughi and Joubert,[9] this extra straining can be denoted by a convergence parameter in simple-convergence boundary layers as

$$\vartheta = -\frac{1}{u}\frac{\partial w}{\partial z} \qquad \text{or} \qquad \vartheta = -\frac{1}{u}\frac{\partial v}{\partial y} \tag{1}$$

depending on orientation, where ϑ is the convergence parameter, u is the streamwise x velocity, and w and v are the spanwise z and normal y velocities, respectively.

This convergence parameter can be included in the momentum-integral equation for boundary layers in the centerline plane as

$$\frac{\mathrm{d}\theta}{\mathrm{d}x} = \frac{C_f}{2} - (H+2)\frac{\theta}{U_1}\frac{\mathrm{d}U_1}{\mathrm{d}x} + \vartheta\theta \tag{2}$$

where θ is the boundary-layer momentum thickness, C_f is the skin-friction coefficient, H is the boundary-layer shape factor, and U_1 is the velocity in the freestream outside the boundary layer. For diverging flows, the sign of the convergence term is reversed.

To quantify the pressure gradients and convergence parameters in the contractions, a numerical solution to the three-dimensional Laplace equation was undertaken for the contractions. The computational scheme is similar to that described by Su,[2] and a full description is given by Callan.[6]

Figure 1 shows the computed pressure distributions along the centerlines and in the corners of the AR 1 and 4 contractions, together with the corresponding ϑ values along the centerlines of the contractions. Here C_p is coefficient of pressure defined as

$$C_p = 1 - (u/U_e)^2 \tag{3}$$

where u is the streamwise velocity along the streamline of interest and U_e is the freestream velocity one effective diameter downstream of the contraction exit.

Figure 1a shows the expected result that two regions of adverse pressure gradient exist on centerlines of the walls: one near the inlet and another near the exit. The pressure history of the AR 1 case (which is the same on all walls due to symmetry) is seen to be markedly different from either of the AR 4 walls. Figure 1b shows that the largest pressure gradient variations occur in the corners, and thus, the points of maximum and minimum velocity in a three-dimensional contraction occur in the corners. Figure 1c shows the strong effect that varying AR has on the convergence parameter. The value of ϑ for AR 1, which due to symmetry is the same on all surfaces, falls between the values of AR 4 floor and AR 4 side wall. The AR 4 case shows that the maximum value of ϑ for the side wall is nearly three times larger than for the floor.

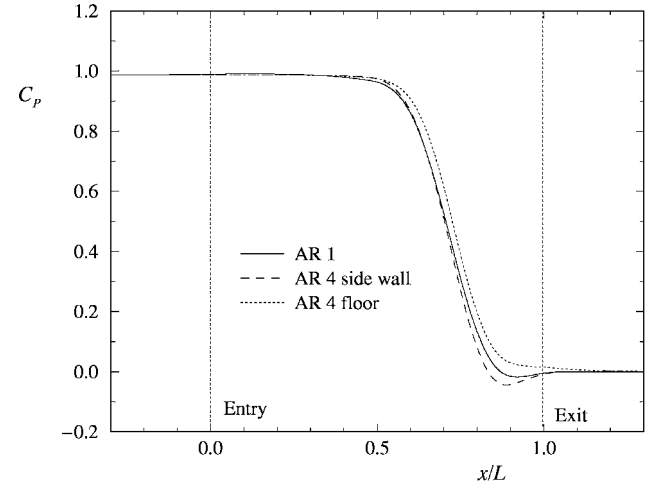

a) Coefficient of pressure along centerlines of side walls and floor

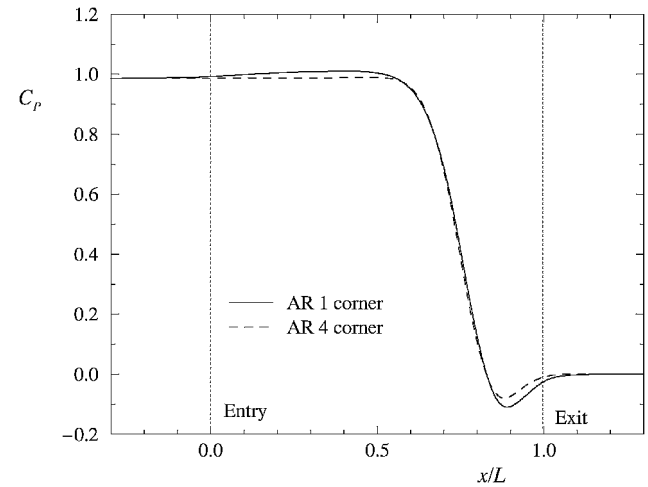

b) Coefficient of pressure along corners

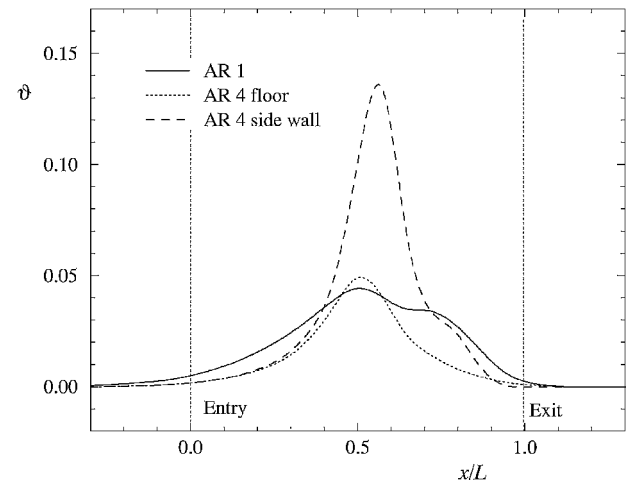

c) Convergence parameter ϑ along centerlines of side walls and floor

Fig. 1 Results of potential flow calculations for AR 1 and 4 cases.

B. Wall Boundary Layers

From Eq. (2), assuming an equivalent streamwise pressure history and skin-friction coefficient between two boundary layers, the phenomenon that controls their development through a contraction is ϑ. However, Fig. 1a shows that the pressure histories between different ARs as well as between the side wall and floor for AR > 1 are different. This illustrates that the boundary-layer developments in a contraction are unique to each particular contraction. Comparisons of exit boundary-layer thicknesses between different ARs is, therefore, not straightforward. However, comparisons of boundary layers within a particular contraction is slightly more straightforward.

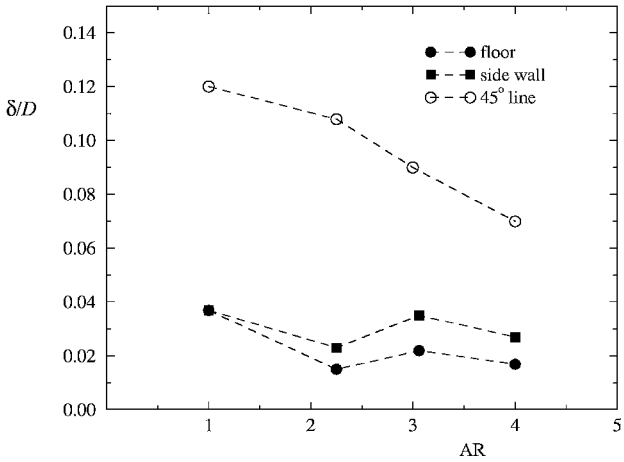

Fig. 2 Boundary-layer thicknesses measured one exit diameter downstream of the exit vs AR.

Figures 1a and 1c show that, for a particular AR, the variation of C_p and ϑ on the side wall and on the floor are both significant, and for AR > 1, the boundary layer on the side wall should be thicker than that on the floor. Note that this reasoning does not consider surface arc lengths. For our study, the lengths of all contractions are fixed ($L = 685$ mm), and for AR 4, the surface length for the floor is no more than 10% longer than the side wall and, therefore, will not have a significant effect.

Figure 2 shows the boundary-layer thicknesses δ along the centerlines of the side wall and floor, respectively (solid symbols), obtained from the mean velocity profiles measured one exit diameter downstream of the exit. Here δ is taken to be δ_{99}, the point at which the mean velocity in the boundary layer is 99% of the freestream mean velocity. The data indicate a general trend of bottom boundary-layer thinning with increasing AR and no clear trend for the side boundary layers. These results highlight that a comparative study of side wall and floor boundary-layer thicknesses between different ARs is not a relative comparison because of the different pressure histories and convergence parameter values. However, a comparison of side boundary-layer thickness vs bottom boundary-layer thickness for a given AR shows that, generally, for AR > 1, $\delta_{\text{side}} > \delta_{\text{floor}}$, as is expected.

C. Corner Boundary Layers

A second feature of interest when examining the effect of AR change in a contraction is the change in corner boundary-layer flow. The variation of C_p through a contraction on the corner, as calculated using the potential flow solution, is shown in Fig. 1b for AR 1 and 4, respectively. It can be seen that both the inlet and exit pressure histories of AR 1 and 4 are different, with AR 1 showing a more pronounced adverse pressure gradient at both inlet and exit. Consequently, one would expect the boundary layer at the corner to be thicker for AR 1 than for AR 4 because of this effect. Measurements of corner boundary-layer thicknesses δ^{45} measured along a 45-deg line, confirm this to be the case, as shown in Fig. 2 (open symbol).

To get a better appreciation of the flow in the corners, mean velocities and turbulence intensities were measured in the lower left hand corner of the exit plane, one exit diameter downstream of exit. Turbulence intensity is defined here as $(\underline{u'^2})^{1/2}/U_e$, where u' is the fluctuating component of streamwise velocity and U_e is the mean freestream velocity. Figure 3 shows contour plots for the AR 4 case. Data were taken with the hot wire normal to the floor for the sections to the right of the diagonal and normal to the side wall for the sections to the left of the diagonal as one views it on the page.

The corner boundary layers are seen to have undergone transition to turbulence, and for this AR 4 case, it is clear that there is no symmetry about the 45-deg line. Figure 4 shows normalized mean velocity profiles along the diagonal of AR 1–4 inclusive, one exit diameter downstream of the exit. The data are seen to collapse fairly well along this diagonal line, and the corner layer is observed to end at about 0.085Γ along this diagonal, where Γ is the diagonal length for a given AR.

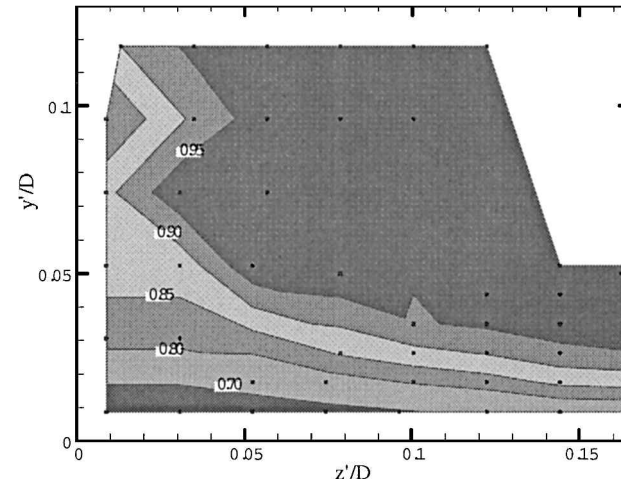

Mean velocity

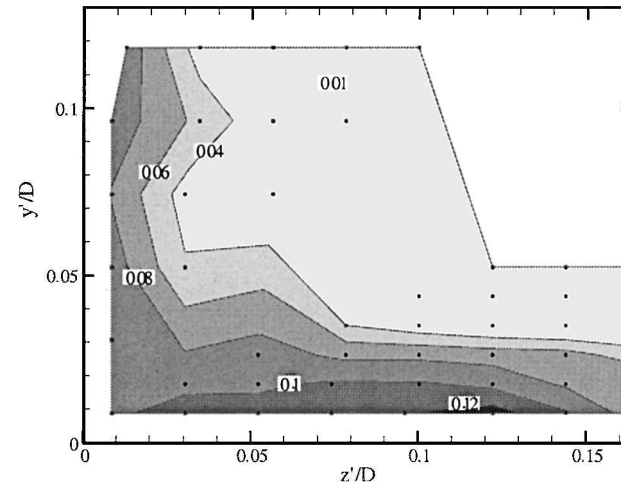

Turbulence intensity

Fig. 3 Contour profiles for AR 4 in corner with origin of the axes in the lower-left-hand corner of the contraction; marked points indicate measurement locations from which contour levels are interpolated.

Previous studies have been conducted on turbulent corner boundary-layer flows. Nakamura et al.,[10] in their experimental study, show the presence of two counter-rotating vortices in a turbulent corner boundary layer aligned either side of the 45-deg line of an arbitrary infinite corner. Because of the small physical size of the boundary layers in the corners in our study, only streamwise velocity measurements were made. In the absence of spanwise and normal component velocity measurements, it is difficult to quantify these vortices. Even so, it is certainly viable to assume the presence, however small, of these counter-rotating vortices in the corner. Furthermore, the results of Fig. 4 would suggest that perhaps the principal orientation of the vortices in the corners of a confined duct is not about the 45-deg line, but is in fact about the diagonal line. The data given here can only suggest that, and further studies would need to be performed.

D. Useful Working Area

Of more practical interest, the results in Fig. 4 can be used as the basis of an approximate design rule for contractions with varying AR. Figure 5 shows a schematic of the useful area of a working section downstream of a contraction exit. Here the useful area is defined as that region where the flow has low freestream turbulence, that is, outside the boundary layers, and has high uniformity across the plane. Hence, it is the area where useful and practical measurements can be made in the working section of a wind tunnel. A simple result follows because along the diagonal the boundary layer ends at

$$C = \lambda/\Gamma = \alpha/W = \beta/H \approx 0.085 \tag{4}$$

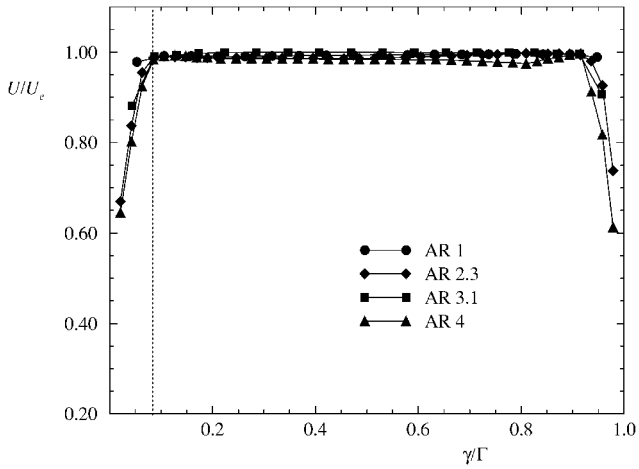

Fig. 4 Diagonal mean velocity profiles.

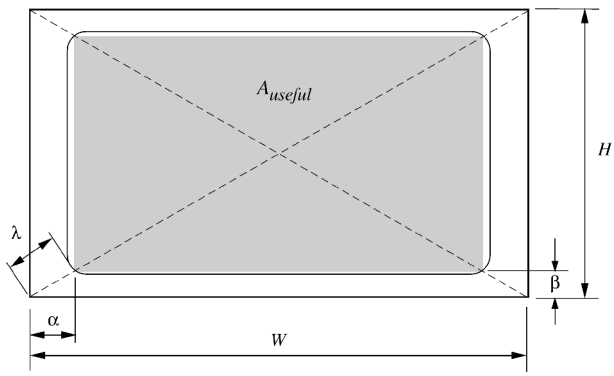

Fig. 5 Useful area of exit plane.

where λ, α, and β are shown in Fig. 5. The total cross-sectional area is $A = WH$, whereas the useful area is defined as $A_{\text{useful}} = (W - 2\alpha)(H - 2\beta)$. When Eq. (4) is used, the useful area becomes

$$A_{\text{useful}} = A(1 - 2C)^2 \approx 0.69A \tag{5}$$

Therefore, the estimated useful cross-sectional working area is a fixed proportion of the total cross-sectional area and has no dependence on AR. Likewise, conservative estimates for useful width and height are also independent of AR: $W_{\text{useful}}/W = H_{\text{useful}}/H \approx 0.83$.

IV. Conclusions

An experimental and computational analysis of the effect of changing the aspect ratio through a three-dimensional wind-tunnel contraction has been performed. Exit flow boundary layers were measured for four contractions ranging from AR 1 to 4, all with equivalent lengths and contraction ratios. Their development was related to the pressure history on the walls, as well as to the related effect of streamline convergence. Comparisons between contractions with different AR show that streamline convergence effects as well as pressure histories need to be considered when performing comparisons of boundary-layer thicknesses on the same wall of the contraction. For a given AR, the side wall boundary layer was found to be thicker than the floor boundary layer for AR > 1. The 45-deg corner boundary-layer thicknesses were found to decrease with increasing AR, consistent with the corner pressure distribution induced by the streamline convergence effects.

An examination of the mean velocity profile along the diagonal of the exit plane reveals a collapse of data. From this, an approximate design rule for the estimation of useful area in the working section has been proposed. For the contraction parameters considered in this study, the useful area is found to be $0.69A$, and this result is independent of AR.

Acknowledgments

The authors were supported by the National Science Foundation through Grants CTS-9983933 and ACI-9982274, and this is gratefully acknowledged.

References

[1]Morel, T., "Comprehensive Design of Axisymmetric Wind Tunnel Contractions," *Journal of Fluids Engineering*, Vol. 97, No. 1, 1975, pp. 225–233.

[2]Su, Y., "Flow Analysis and Design of Three-Dimensional Wind Tunnel Contractions," *AIAA Journal*, Vol. 29, No. 11, 1991, pp. 1912–1920.

[3]Mikhail, M. N., "Optimum Design of Wind-Tunnel Contractions," *AIAA Journal*, Vol. 17, No. 5, 1979, pp. 471–477.

[4]Fang, F. M., "Design Method for Contractions with Square End Sections," *Journal of Fluids Engineering*, Vol. 119, No. 2, 1997, pp. 454–458.

[5]Tulapurkara, E. G., and Bhalla, V. V. K., "Experimental Investigation of Morel's Method for Wind Tunnel Contractions," *Journal of Fluids Engineering*, Vol. 110, No. 1, 1988, pp. 45–47.

[6]Callan, J., "The Effect of a Changing Aspect Ratio Through a Wind Tunnel Contraction," M.S. Thesis, Aerospace Engineering, Univ. of Minnesota, Minneapolis, MN, 2000.

[7]Zamir, M., and Young, A. D., "Experimental Investigation of the Boundary Layer in a Streamwise Corner," *Aeronautical Quarterly*, Vol. 21, Nov. 1970, pp. 313–339.

[8]Bradshaw, P., "Effects of Streamline Curvature on Turbulent Flow," AG-169, AGARD, 1973.

[9]Saddoughi, S. G., and Joubert, P. N., "Lateral Straining of Turbulent Boundary Layers. Part 1. Streamline Divergence," *Journal of Fluid Mechanics*, Vol. 229, 1991, pp. 173–204.

[10]Nakamura, I., Miyata, M., Kushida, T., and Kagiya, Y., "An Experimental Study of the Intermittant Region of a Corner Turbulent Boundary Layer," *Japan Society of Mechanical Engineers International Journal*, Vol. 30, No. 259, 1987, pp. 72–79.

A. Plotkin
Associate Editor

New ν_t–k Model for Calculation of Wall-Bounded Turbulent Flows

Seong Hoon Kim* and Myung Kyoon Chung†
Korea Advanced Institute of Science and Technology, Taejon 305-701, Republic of Korea

Introduction

HISTORICALLY, the Boussinesq eddy viscosity that is assumed for Reynolds shear stress has been indirectly assessed by estimating the velocity scale and length scale of turbulent energetic eddies. Physical models to find these scales were the mixing length model,[1] the one-equation model employing the k equation of Bradshaw et al.,[2] and the two-equation model using the k–ε equations of Jones and Launder[3] or the k–ω equations of Wilcox.[4] More recently, the one-equation model has reemerged by Baldwin and Barth[5] and Spalart and Allmaras.[6] Instead of the k equation, however, they proposed to solve the ν_t equation to assess directly the eddy viscosity. Subsequently, Durbin et al.[7] and Menter[8] formulated other forms of ν_t equations.

To avoid the problem in the one-equation model that the length scale needs to be provided externally, these one-equation models use the von Kármán length scale, $L_{vK} \equiv |S/\nabla S|$, where S is the mean rate of strain, or a composite length scale,[7] ($|\nabla \nu_t/S|$). Because of the advantages of directness of eddy viscosity assessment, simplicity in numerical computation, and use of natural boundary condition for the ν_t equation, the one-equation model has often been a preferred choice in aerodynamic calculations. However, such one-equation models have the following three serious problems. One is that the length scale defined in any of the two methods mentioned earlier varies physically unrealistically in both the near-wall layer and the core region. The second problem is that predicted ν_t varies as y^4 as $y \to 0$ (Fig. 1). The third problem is that when the one-equation

Received 28 November 2000; revision received 23 April 2001; accepted for publication 14 May 2001.

*Graduate Student, Department of Mechanical Engineering, 373-1, Kusong-dong, Yusong-gu.

†Professor, Department of Mechanical Engineering, 373-1, Kusong-dong, Yusong-gu.